Inorganic Chemistry

Article

pubs.acs.org/IC

$A_5Sn_2As_6$ (A = Sr, Eu). Synthesis, Crystal and Electronic Structure, and Thermoelectric Properties

Jian Wang, Sheng-Qing Xia,* and Xu-Tang Tao*

State Key Laboratory of Crystal Materials, Institute of Crystal Materials, Shandong University, Jinan, Shandong 250100, People's Republic of China

Supporting Information

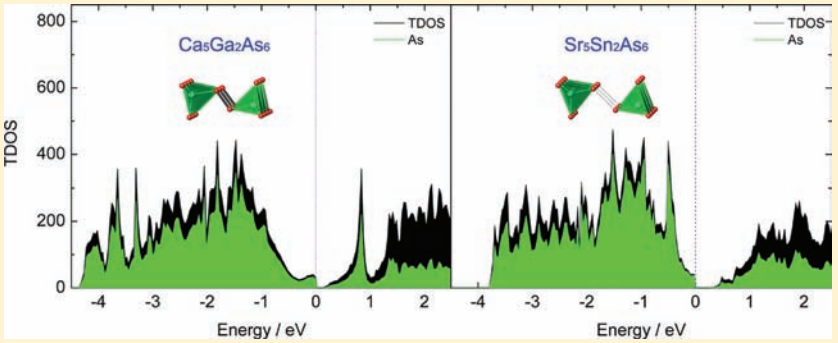

ABSTRACT: Two new ternary Zintl phases, $Sr_5Sn_2As_6$ and $Eu_5Sn_2As_6$, have been synthesized, and their structures have been accurately determined through single-crystal X-ray diffraction. Both compounds crystallize in orthorhombic space group *Pbam* (No. 55, $Z = 2$) with cell parameters of $a = 12.482(3)/12.281(5)$ Å, $b = 14.137(3)/13.941(5)$ Å, and $c = 4.2440(10)/4.2029(16)$ Å for $Sr_5Sn_2As_6$ (R1 = 0.0341; wR2 = 0.0628) and $Eu_5Sn_2As_6$ (R1 = 0.0324; wR2 = 0.0766), respectively. Their structure belongs to the $Sr_5Sn_2P_6$ type, which can be closely related to the $Ca_5Ga_2As_6$ type. Electronic band structure calculations based on the density functional theory reveal an interesting electronic effect in the structure formation of these two types of Zintl phases, which substantially affect their corresponding electronic band structure. Related studies on the thermal stability, magnetism, and thermoelectric properties of $Eu_5Sn_2As_6$ are presented as well.

INTRODUCTION

In the past decades, studies on the intermetallic compounds and Zintl phases have always been at the forefront of scientific research. The complex relationships between their crystal structure, chemical bonding, electronic structure, and physical properties are especially of interest to the solid-state chemists, and extensive attention has been attracted concerning these issues.[1−7] For classical Zintl phases, the system resembles the typical valence compounds, and a simple reasoning by treating the cations as "electron donors" and the anions as "electron acceptors" usually works satisfactorily in rationalizing the electronic structure.[8−10] Such a notion also suggests normally that the electronic requirements should be the dominating factor in governing the formation of Zintl phases.

More interestingly, complex Zintl phases can often lead to unusual electronic structure and abundant physical properties. Especially, exploration of new thermoelectric candidates within the Zintl realm is of great interest. For example, high thermoelectric efficiency has been demonstrated by a number of Zintl phases such as Ca_3AlSb_3,[11] $Ca_5Al_2Sb_6$,[12] $Ba_8Ga_{16}Ge_{30}$,[13] $YbZn_2Sb_2$,[14] and $Yb_{14}MnSb_{11}$.[15] The excellent performance of these new thermoelectric materials has been proven to benefit from their complex crystal structure and unique electronic structure, which can possess either high electronic mobility or low lattice thermal conductivity.[13−15] Among these materials, $Ca_5Al_2Sb_6$ has been considered as a new low-cost and highly efficient thermoelectric candidate, and especially with its carrier concentration optimized by blending Na or Zn, a high figure of merit ($zT > 0.6$) can be achieved at 1000 K.[12,16]

In previous work, we have thoroughly explored the A−Cd−Pn system (A = divalent alkaline-earth or rare-earth elements such as Ca, Sr, Eu, and Ba; Pn = As, P) and reported a number of new ternary Zintl phases that exhibit semiconducting properties.[17] The title compound $Eu_5Sn_2As_6$ was serendipitously synthesized from an experiment aimed at optimizing the crystal growth of Eu_2CdAs_2 in Sn flux. After its crystal structure was accurately identified, the product was reproduced by excluding Cd from the reaction. For the A−Sn−As system, there have been rich structural types reported, which are represented by several typical compounds such as $SrSn_2As_2$,[18,19] $Ba_3Sn_4As_6$,[20] $Ba_3Sn_2As_6$,[21] and $Ca_5Sn_2As_6$.[22] Here we report the synthesis, property, and crystal and electronic structure of two new ternary Zintl phases, $Sr_5Sn_2As_6$ and $Eu_5Sn_2As_6$. The structure of these two compounds belongs to the orthorhombic $Sr_5Sn_2P_6$ type.[23] Although such a structure type has been

Received: February 11, 2012
Published: May 7, 2012

   dx.doi.org/10.1021/ic300308w | Inorg. Chem. 2012, 51, 5771−5778

discovered for more than 20 years, only two compounds, $Sr_5Sn_2P_6$[23] and $Ca_5Sn_2As_6$,[22] have appeared in references, and no properties have been reported on these phases so far. In this paper, the close relationship between $Sr_5Sn_2As_6$ and $Ca_5Ga_2As_6$ about their crystal and electronic band structure is discussed by incorporating density functional theory calculations. Studies on related thermal stability, magnetism, and thermoelectric properties are presented as well.

EXPERIMENTAL SECTION

Synthesis. All syntheses were performed inside an argon-filled glovebox with oxygen and moisture levels below 0.1 ppm or under vacuum. The starting materials were commercially purchased and used as received: Eu (Alfa, rod, 99.9% metal basis), Sr (Alfa, granules, 99% metal basis), Sn (Alfa, granules, 99.9% metal basis), and As (Alfa, Lump, 99.999%). Single crystals of $Eu_5Sn_2As_6$ and $Sr_5Sn_2As_6$ can both be grown by metal-flux reactions utilizing Sn as self-flux. The optimized synthesis procedure can be described as follows: A (Eu or Sr), Sn, and As in a molar ratio of A:Sn:As = 1:15:1 were loaded into an alumina crucible, which was subsequently flame-sealed in an evacuated fused silica jacket. The reaction mixture was first heated from 100 to 900 °C at a rate of 200 °C/h, homogenized at this temperature for 24 h, and then slowly cooled to 600 °C at a rate of 2 °C/h. At this temperature, the ampule was quickly taken out of the furnace, inverted, and spun in a centrifuge to remove the excess of Sn. The products are shiny, black, and needlelike crystals of the title compounds with high purity. Compound $Eu_5Sn_2As_6$ showed good stability in air; however, the crystals of $Sr_5Sn_2As_6$ decomposed quickly when exposed to air or moisture.

Single-Crystal X-ray Diffraction and Structure Determination. In order to avoid possible decomposition of the title compounds during the data collection, all crystals were picked in an argon-filled glovebox and cut in Paratone N oil to the desired dimensions. The data collections were carried out under the protection of an inert atmosphere, achieved by using a nitrogen gas stream. Preliminary lattice parameters and orientation matrices were obtained from three sets of frames. Data reduction and integration, together with global unit cell refinements, were done by the *INTEGRATE* program of the *APEX2* software.[24] Semiempirical absorption corrections were applied using the *SCALE* program for the area detector.[24] The structures were solved by direct methods and refined by full-matrix least-squares methods on F^2 using *SHELX*.[25] In the last refinement cycles, the atomic positions were standardized using the program *STRUCTURE TIDY*.[26,27] All structures were refined to convergence with anisotropic displacement parameters.

Details of the data collection and structure refinement are provided in Table 1. Positional and equivalent isotropic displacement parameters and important bond distances are listed in Tables 2 and 3, respectively. Further information in the form of CIF has been deposited with Fachinformationszentrum Karlsruhe, 76344 Eggenstein-Leopoldshafen, Germany [fax (49) 7247-808-666; e-mail crysdata@fiz-karlsruhe.de] as depository CSD numbers 424070 for $Sr_5Sn_2As_6$ and 424071 for $Eu_5Sn_2As_6$, respectively.

Powder X-ray Diffraction. For phase identification, powder X-ray diffraction patterns were taken at room temperature by a Bruker AXS X-ray powder diffractometer using Cu Kα radiation. Because of the air sensitivity of $Sr_5Sn_2As_6$, only $Eu_5Sn_2As_6$ was chosen for study and the data were recorded in a 2θ mode with a step size of 0.02° and a counting time of 10 s. The measured and calculated patterns of $Eu_5Sn_2As_6$ were in good agreement on the positions of the Bragg reflections, and their intensity difference indicates the existence of preferred orientations of the powder sample (Supporting Information).

Differential Thermal Analysis and Thermogravimetric Analysis (DTA/TGA) Measurements. With consideration of a possible thermoelectric application, the thermal stability of $Eu_5Sn_2As_6$ was tested using a Mettler-Toledo TGA/DSC/1600HT instrument. TGA and differential scanning calorimetry (DSC) experiments were performed on a polycrystalline sample of $Eu_5Sn_2As_6$ (26.58 mg), and data were taken under the protection of high-purity argon gas. A temperature range from 300 to 1400 K was applied with a heating rate of 10 °C/min.

Magnetic Susceptibility. Field-cooled direct-current (dc) magnetization measurements on the polycrystalline sample of $Eu_5Sn_2As_6$ (33.6 mg) were conducted in a Quantum Design MPMS SQUID magnetometer. The applied magnetic field H was 1000 Oe, and the temperature interval was 4–300 K. The raw data were corrected for the holder's diamagnetic contribution and converted to molar susceptibility.

Sample Preparation for Thermoelectric Property Measurements. Single crystals of $Eu_5Sn_2As_6$ were prepared through Sn-flux reactions as described above. The crystals with a mass of about 2.5 g were ground into fine powder and then sintered through spark plasma sintering (SPS 1050: Sumitomo Coal Mining Co., Ltd.) at 700 °C for about 10 min with a uniaxial pressure of 30 MPa. The resulting pellets (Ø 12.7 × 2.5 mm^2) were carefully cleaned and polished in the glovebox to avoid possible surface contamination. The densities (calculated from measured dimensions and weight) were found to be

Table 1. Selected Crystal Data and Structure Refinement Parameters for $Sr_5Sn_2As_6$ and $Eu_5Sn_2As_6$

formula	$Sr_5Sn_2As_6$	$Eu_5Sn_2As_6$
fw/(g/mol)	1125.00	1446.70
T/°C	−123	−123
radiation, wavelength	Mo Kα, 0.71073 Å	
space group, Z	*Pbam* (No. 55), 2	*Pbam* (No. 55), 2
unit cell dimensions		
a/Å	12.482(3)	12.281(5)
b/Å	14.137(3)	13.941(5)
c/Å	4.2440(10)	4.2029(16)
V/Å^3	748.9(3)	719.6(5)
ρ_{calc}/(g/cm^3)	4.989	6.677
$\mu_{Mo\ K\alpha}$/mm^{-1}	34.061	38.503
final R indices[a] [$I > 2\sigma(I)$]	R1 = 0.0341, wR2 = 0.0628	R1 = 0.0324, wR2 = 0.0766
final R indices[a] [all data]	R1 = 0.0598, wR2 = 0.0710	R1 = 0.0432, wR2 = 0.0818

[a] $R1 = \sum||F_o| - |F_c||/\sum|F_o|$; $wR2 = [\sum[w(F_o^2 - F_c^2)^2]/\sum[w(F_o^2)^2]]^{1/2}$, where $w = 1/[\sigma^2F_o^2 + (AP)^2 + BP]$, with $P = (F_o^2 + 2F_c^2)/3$; A and B are weight coefficients.

Table 2. Refined Atomic Coordinates and Isotropic Displacement Parameters for $Sr_5Sn_2As_6$ and $Eu_5Sn_2As_6$

atom	Wyckoff position	x	y	z	U_{eq} (Å^2)
		$Sr_5Sn_2As_6$			
Sr1	4g	0.12106(9)	0.24155(8)	0	0.0127(3)
Sr2	4g	0.37091(10)	0.06835(8)	0	0.0130(3)
Sr3	2a	0	0	0	0.0119(4)
Sn1	4h	0.28548(7)	0.39549(6)	1/2	0.0112(2)
As1	4h	0.07675(10)	0.39704(10)	1/2	0.0129(3)
As2	4h	0.17039(11)	0.07710(8)	1/2	0.0116(3)
As3	4g	0.36831(10)	0.30433(9)	0	0.0116(3)
		$Eu_5Sn_2As_6$			
Eu1	4g	0.12295(5)	0.24214(5)	0	0.0126(2)
Eu2	4g	0.37082(6)	0.06677(5)	0	0.0137(2)
Eu3	2a	0	0	0	0.0126(3)
Sn1	4h	0.28704(8)	0.39412(6)	1/2	0.0119(2)
As1	4h	0.07533(12)	0.39566(10)	1/2	0.0126(3)
As2	4h	0.17012(13)	0.07820(10)	1/2	0.0121(3)
As3	4g	0.37085(11)	0.30188(10)	0	0.0126(3)

[a] U_{eq} is defined as one-third of the trace of the orthogonalized U^{ij} tensor.

dx.doi.org/10.1021/ic300308w | Inorg. Chem. 2012, 51, 5771−5778

Table 3. Important Interatomic Distances (Å) in $Sr_5Sn_2As_6$ and $Eu_5Sn_2As_6$

atom pair	distance (Å)	atom pair	distance (Å)
	$Sr_5Sn_2As_6$		
Sr1–As1×2	3.1049(14)	Sr2–As1×2	3.2856(15)
As2×2	3.2073(13)	As1×2	3.3681(15)
As3	3.2112(19)	As2×2	3.2837(15)
As3	3.2208(19)	As3	3.3362(19)
Sr3–As2×4	3.1959(11)		
As3×2	3.2178(14)		
Sn1–As1	2.6054(17)		
As2	2.6259(16)		
As3×2	2.6894(10)		
	$Eu_5Sn_2As_6$		
Eu1–As1×2	3.0560(14)	Eu2–As1×2	3.2471(14)
As2×2	3.1584(14)	As1×2	3.3165(15)
As3	3.1564(19)	As2×2	3.2430(15)
As3	3.1565(19)	As3	3.278(2)
Eu3–As2×4	3.1575(14)		
As3×2	3.1851(17)		
Sn1–As1	2.600(2)		
As2	2.6198(19)		
As3×2	2.6701(12)		

about 97% of the theoretical density. Powder X-ray diffraction experiments on samples before and after SPS treatment proved to show identical phases (Supporting Information).

Seebeck Coefficient and Resistivity Measurements. After the thermal conductivity measurements were done, the sample pellets were cut into bars with suitable dimensions (12.5 × 2.5 × 2.4 mm^3) for the Seebeck coefficient and electrical resistivity measurements. These two parameters were measured simultaneously in a temperature range from 300 to 780 K under a He atmosphere by using a ULVAC-RIKO ZEM-3 instrument system.

Thermal Conductivity Measurements. The thermal conductivity was measured on a disk sample (Ø 12.7 × 2.01 mm^2) of $Eu_5Sn_2As_6$ in a flowing Ar atmosphere by using the NETZSCH LFA457 instrument. The measurements were performed in a temperature range from room temperature to 720 K, and a pyroceram 9606 (Ø 12.7 × 1.98 mm^2) standard sample was used as the reference.

Figure of Merit Calculations. The temperature dependences of the resistivity and Seebeck coefficient data were fit using third- and sixth-order polynomial curves, respectively. Calculations of the figure of merit were carried out according to ref 28.

Computational Details. To better understand the structure relationship between these new phases and their closely related analogues, electronic band structure calculations were performed on $Sr_5Sn_2As_6$ and $Ca_5Ga_2As_6$, respectively. The full-potential linearized augmented plane-wave method (FP-LAPW)[29,30] was applied with the aid of the *Wien2k* code.[31] In this method, the unit cell is divided into nonoverlapping muffin-tin (MT) spheres and an interstitial region. The wave functions in the interstitial regions are expanded in plane waves up to $R_{MT} \times K_{max} = 7$, where R_{MT} is the smallest radius of all MT spheres and K_{max} the plane-wave cutoff. The valence wave functions inside the MT spheres are expanded up to $l_{max} = 10$, while the charge density was Fourier-expanded up to $G_{max} = 12$ au^{-1}. The MT radii were chosen to be 2.5 bohr for both Ca and Sr atoms, 2.45 bohr for Sn atoms, and 2.33 bohr for both Ga and As atoms. The exchange correlation potential was calculated using the Perdew–Burke–Ernzerhof generalized gradient approximation.[32] Self-consistency was achieved using 1000 *k* points in the irreducible Brillouin zone (BZ). The BZ integration was performed using the tetrahedron method, and the self-consistent calculations were considered to have converged if the total energy and charge of the system are stable within 10^{-4} Ryd and 10^{-4} e^-, respectively.

Besides, various bonding interactions in both $Ca_5Ga_2As_6$ and $Sr_5Sn_2As_6$ were calculated and compared. This was done by using the linear muffin-tin orbital (LMTO) method,[33−37] as implemented in the program *LMTO 4.7*.[38] In this case, exchange and correlation were treated in a local density approximation,[39] and all relativistic effects except for spin–orbit coupling were taken into account by a scalar relativistic approximation.[40] To achieve the space filling, interstitial spheres were inserted automatically.[41] The basis set included 4s, 4p, and 3d for Ca, 5s, 5p, and 4d for Sr, 4s, 4p, and 4d for Ga, 5s, 5p, and 5d for Sn, and 4s, 4p, and 4d for As. The Ca 4p, Sr 5p, Ga 4d, Sn 5d, and As 4d orbitals were all treated with downfolding techniques.[42] The *k*-space integrations were performed by the tetrahedron method,[43] and a total of 1440 *k* points in the BZ were used. The Fermi level was selected as the energy reference in all calculations.

RESULTS AND DISCUSSION

Structure Description. For compounds forming with the nominal $A_5M_2Pn_6$ formula (A = divalent alkaline-earth or rare-earth metals; M = triels or tetrels; Pn = pnictogen elements), there have been three structure types reported in the references, which are represented by $Ca_5Ga_2As_6$,[44] $Ba_5Al_2Bi_6$,[45,46] and $Sr_5Sn_2P_6$,[23] respectively. The former two structures highly resemble each other except for the different coordination geometries for one of the cations: for the $Ca_5Ga_2As_6$ structure type, the cation is in an ideal octahedral geometry, while for the $Ba_5Al_2Bi_6$ structure type, it is in a distorted octahedral geometry. However, the structure of $Sr_5Sn_2P_6$ is subtly different from those of $Ca_5Ga_2As_6$ or $Ba_5Al_2Bi_6$ in the polyanionic chains. The newly discovered compounds $Sr_5Sn_2As_6$ and $Eu_5Sn_2As_6$ both crystallize in the $Sr_5Sn_2P_6$ structure type, and because this structure has been reported in a previous reference, here we will only choose $Sr_5Sn_2As_6$ for a brief discussion, and the description will be mainly focused on its relationship to the $Ca_5Ga_2As_6$ type.

The electron counting of $Sr_5Sn_2As_6$ can be understood through the Zintl–Klemm concept.[8−10] With the formal oxidation states assigned as Sr^{2+}, Sn^{4+}, and As^{3-}, the compound is typically a charge-balanced Zintl phase. A polyhedral representation of the structure of $Sr_5Sn_2As_6$ is provided in Figure 1. The polyanionic structure of $Sr_5Sn_2As_6$ features one-dimensional chains running in the *c* direction, which are

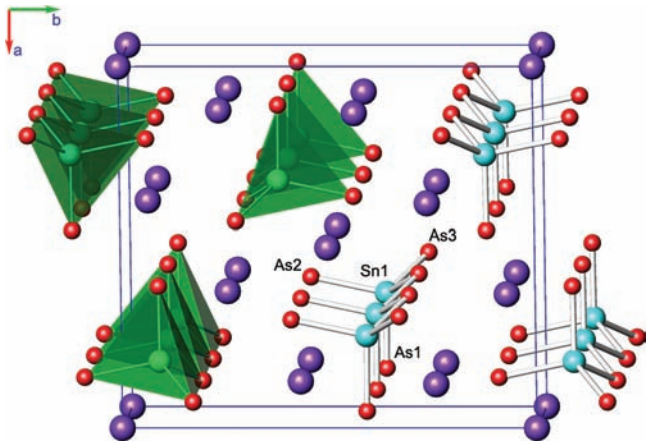

Figure 1. Polyhedral and ball-and-stick representation of the structure for $Sr_5Sn_2As_6$. The Sn atoms at the centers of the translucent As tetrahedra are drawn as light-blue spheres, and the As atoms are plotted as red spheres. The Sr cations filling the cavities among the $[Sn_2As_6]$ chains are indicated as purple spheres. The structure is projected along the *c* axis, and the unit cell is outlined.

dx.doi.org/10.1021/ic300308w | Inorg. Chem. 2012, 51, 5771−5778

constructed of all corner-shared $SnAs_4$ tetrahedra. A similar chain structure has also been observed in other types of Zintl phases, such as Ca_3InP_3[47] and Ba_2MnS_3.[48,49] There are in total three crystallographically independent Sr^{2+} cations: one of them, namely, Sr2, is coordinated to seven As^{3-} anions, and the other two are in a distorted octahedral geometry surrounded by six As atoms. The bonding distances between Sr and As atoms range from 3.1049(14) to 3.3681(15) Å, which are comparable to those of previously reported strontium arsenides, such as Sr_2CdAs_2,[17] $SrCd_2As_2$,[50] and so on. Details on various bonding interactions of $Sr_5Sn_2As_6$ and $Eu_5Sn_2As_6$ are tabulated in Table 3.

One very interesting aspect about these phases worthy of special discussion here is the close structural relationship between the $Ca_5Ga_2As_6$ and $Sr_5Sn_2As_6$ types. A schematic comparison on their polyanion structures are presented in Figure 2. As seen from the graph, both types feature one-

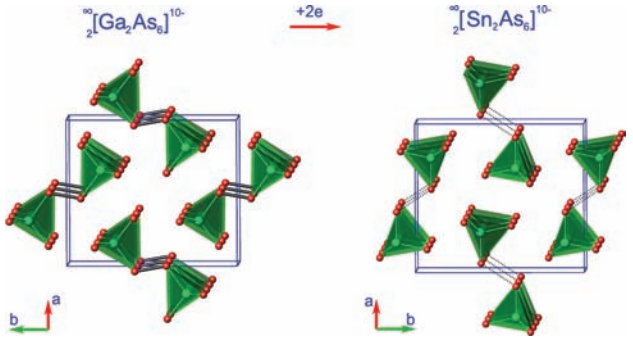

Figure 2. Structural relationship between the $[Ga_2As_6]$ and $[Sn_2As_6]$ polyanion chains. For a better comparison, some specific As atoms among the $[Sn_2As_6]$ chains are linked on purpose by dashed lines. See the text for details.

dimensional chain structures based on corner-shared MAs_6 tetrahedra (M = Ga or Sn). The major discrepancy lies in the polyanion chains: For $[Ga_2As_6]^{10-}$, there exist As−As dimers bridging two $[GaAs_3]$ single chains and thus a double-chain structure forms, whereas for $[Sn_2As_6]^{10-}$, the polyanion can be viewed as two discrete $[SnAs_3]$ chains and no evidential As−As bonds can be identified in the structure. However, by hypothetical linking of some specific As1 atoms in $[Sn_2As_6]^{10-}$, as illustrated by black dashed lines in Figure 2, the polyanion structures of these two different types exhibit exactly identical topology. The above results are easily understood just by applying a simple electron counting, and their formulas can be simply rationalized as $[Ca^{2+}]_5[Ga^{3+}]_2[As^{2-}]_2[As^{3-}]_4$ and $[Sr^{2+}]_5[Sn^{4+}]_2[As^{3-}]_6$. Thus, the bond breaking and structure formation of the $Sr_5Sn_2As_6$ series are actually dominated by the electronic effect.

It is also interesting to compare the results above with the previous studies on the $A_{21}Cd_4Pn_{18}$ series (A = Sr, Eu, Ba; Pn = Sb, Bi), for which similar structural variation has also been reported.[51] However, in the case of $A_{21}Cd_4Pn_{18}$, the size effect takes priority over the electronic effect; i.e., $Sr_{21}Cd_4Bi_{18}$ and $Ba_{21}Cd_4Sb_{18}$ crystallize in different space groups because of different polyanion structures: the former, with the structure type of $Sr_{21}Mn_4Sb_{18}$,[52] contains the anion cluster identified as $[Cd_8Sb_{22}]^{48-}$, whereas in the latter, if bigger cations Ba^{2+} are used, a breakdown of the polyanion results in two isolated $[Cd_4Sb_{12}]^{26-}$ units and, unlike the $A_5M_2Pn_6$ series, this bond breaking is not associated with the pnictogen dimers.[51] Such considerations further raise a new question: Why does the bond breaking in $A_5M_2Pn_6$ take place through the pnictogen dimers? Apparently, this question cannot be answered just by a simple Zintl reasoning described above. Thus, it is necessary to proceed to careful calculation on the $A_5M_2Pn_6$ system. Two compounds, $Ca_5Ga_2As_6$ and $Sr_5Sn_2As_6$, which typically represent the two different structure types, are chosen for such studies, and the results are presented as below.

Magnetic Susceptibility. As seen in Figure 3, compound $Eu_5Sn_2As_6$ exhibits paramagnetic behavior above 30 K and a fit

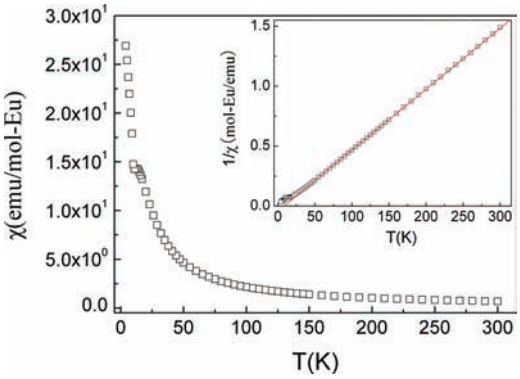

Figure 3. Temperature-dependent magnetic susceptibility measurements for $Eu_5Sn_2As_6$. The data were collected upon cooling from 300 to 4 K at a field of 1000 Oe, and the inverse susceptibility as a function of the temperature and a linear fit to the Curie−Weiss law were also indicated.

of this portion of data to the Curie−Weiss law $\chi(T) = C/(T - \theta)$, where χ means the molar susceptibility, C represents the Curie constant ($C = N_A\mu_{eff}^2/k_B$), and θ is the Weiss temperature, yields an effective moment of 7.93 μ_B per Eu atom, which perfectly matches the theoretical moment of the divalent Eu^{2+} cation. The weak ferromagnetic coupling of Eu 4f spins is suggested by a small positive Weiss temperature of ~8 K, as indicated in the inset by the plot of inverse molar susceptibility versus temperature. These results support the above electron counting on the $Sr_5Sn_2As_6$ system and are consistent with previous reports on related europium arsenide or phosphide Zintl analogues, such as Eu_2CdAs_2,[17] $EuGa_2P_2$,[52] and $EuGa_2As_2$.[53]

Electronic Structure. The calculated band structures of $Ca_5Ga_2As_6$ and $Sr_5Sn_2As_6$ are compared side-by-side in Figure 4. It is not unexpected that these two compounds show high similarities in their band structures. Along the lines $\Gamma \rightarrow Z$ or $\Gamma \rightarrow R$, all bands have relatively large dispersions; however, inside the XY plane, their bandwidths become much narrower. According to the theoretical estimation, both compounds seem to be narrow-band-gap (about 0.2 eV) semiconductors. These results are consistent with previous investigations on $Ca_5Al_2Sb_6$[12] and are also supported by the resistivity measurements on $Eu_5Sn_5As_6$ as below.

One very interesting aspect worthy of more discussion here is that the positions of the Fermi level in the band structures are subtly different in these two compounds. For $Ca_5Ga_2As_6$, there are two relatively narrow bands above the Fermi level, as plotted in black and green lines in the graph. However, for $Eu_5Sn_2As_6$, these two bands are no longer empty and become the top of the valence band. This phenomenon is not difficult to understand. Each unit cell of $Eu_5Sn_2As_6$ contains four more valence electrons than that of $Ca_5Ga_2As_6$, which means two

dx.doi.org/10.1021/ic300308w | Inorg. Chem. 2012, 51, 5771−5778

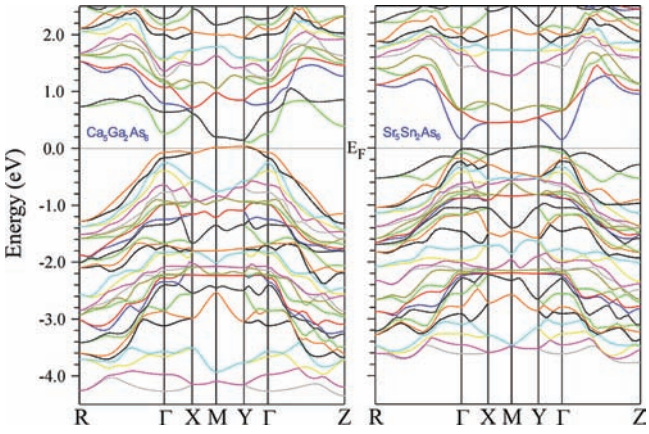

Figure 4. Calculated electronic band structures for $Ca_5Ga_2As_6$ and $Sr_5Sn_2As_6$, respectively. The Fermi level is chosen as the energy reference at 0 eV.

more bands will be filled in order to accept these additional electrons in $Eu_5Sn_2As_6$. The calculated total and projected density of states (DOS) can provide more information in helping to understand these results. As indicated in Figure 5, the DOS of $Ca_5Ga_2As_6$ in the vicinity of the Fermi level are mostly contributed by the As atoms, specifically by the p orbitals of As1, which leads to a sharp peak above the Fermi level and a small shoulder peak below the Fermi level. In the case of $Sr_5Sn_2As_6$, a similar situation is observed except that the

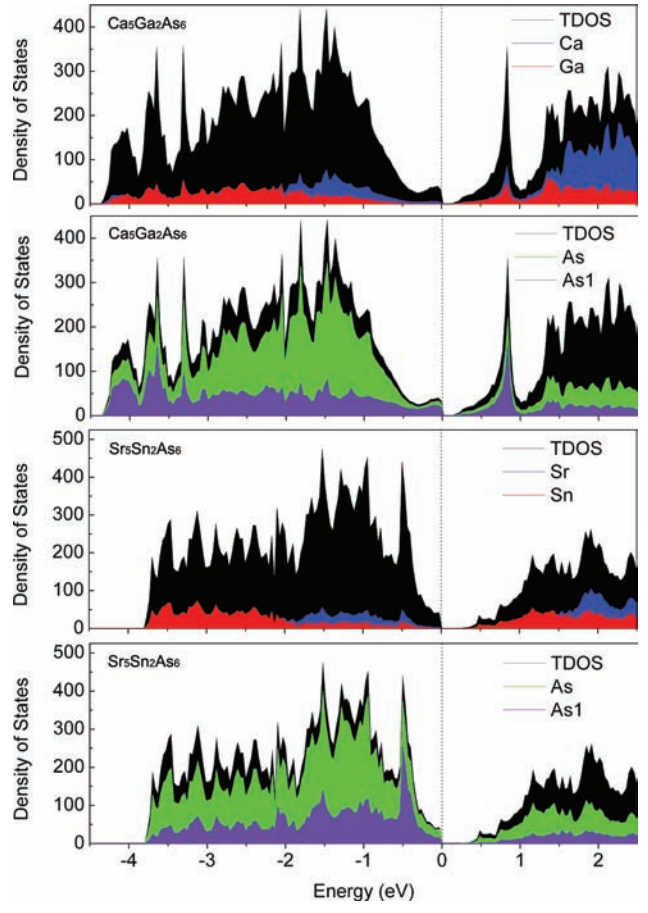

Figure 5. Calculated total and projected DOS for $Ca_5Ga_2As_6$ and $Sr_5Sn_2As_6$.

peaks corresponding to the p orbitals of As1 almost all locate below the Fermi level (Figure 5).

To better understand the electronic effect and structural relationship between the $Ca_5Ga_2As_6$ and $Sr_5Sn_2As_6$ types, various interatomic interactions were calculated, and the results are presented in Figure 6. For compound $Ca_5Ga_2As_6$, the

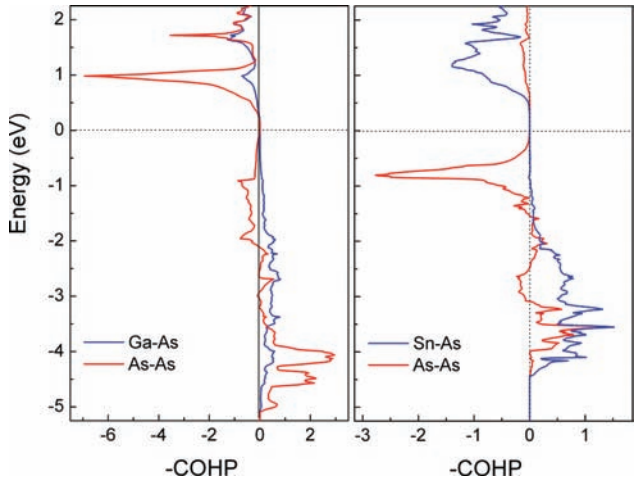

Figure 6. Calculated COHP of various interatomic interactions for $Ca_5Ga_2As_6$ (left) and $Sr_5Sn_2As_6$ (right).

crystal orbital Hamilton population (COHP) of the As−As bond shows strong σ-bonding and σ^*-antibonding interactions in two energy regions, which are from −3.8 to −5.1 eV and from 0.3 to 1.3 eV, respectively. The relatively weaker π-bonding and π^*-antibonding contributions both populate below the Fermi level, confirming single-bond character of the arsenic dimers. The Ga−As pairs of $Ca_5Ga_2As_6$ show very different COHP curves, in which both bonding and antibonding interactions seem much more dispersive. These results can provide an explanation of why the As−As bonds are more fragile. When excessive electrons are introduced, they will be filled into their strong antibonding orbitals. Similar calculations on compound $Sr_5Sn_2As_6$ can further illustrate this point, and with the antibonding orbitals filled, the overall contributions between the As atoms are basically nonbonding with an almost zero integrated COHP (iCOHP) value of 0.026 Ry/cell, whereas the Sn and As atoms are still covalently bonded and the corresponding average iCOHP value is −0.201 Ry/cell.

Thermal Stability. Compound $Eu_5Sn_2As_6$ started to decompose irreversibly above 1250 K, and no significant melting or phase-transition processes were observed below the decomposition temperature according to the DTA/DSC data presented in Figure 7. Two small endothermic peaks, appearing at around 505 and 1050 K in the DSC curve, respectively, can be designated as thermal behavior related to some trace impurities; the former is in exact agreement with the melting point of Sn.

Thermoelectric Properties. The electrical resistivity and Seebeck coefficient for $Eu_5Sn_2As_6$ were measured simultaneously on a polycrystalline sample prepared through the SPS technique described above, and the results are presented in Figure 8. The room temperature resistivity of $Eu_5Sn_5As_6$ is about 280 mΩ·cm, and with increasing temperature, the resistivity decreases dramatically and achieves 25 mΩ·cm at 725 K. This behavior indicates that compound $Eu_5Sn_5As_6$ is a

dx.doi.org/10.1021/ic300308w | Inorg. Chem. 2012, 51, 5771−5778

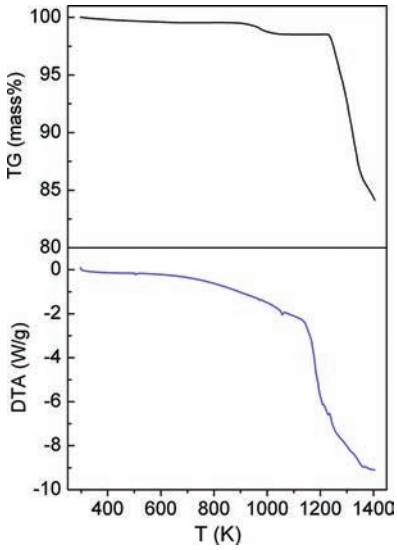

Figure 7. TGA/DSC measurements on $Eu_5Sn_2As_6$, performed under the protection of an Ar gas stream in the temperature range from 300 to 1400 K. Decomposition takes place above 1250 K, and no melting or phase-transition processes are observed. Below this temperature, a small weight loss may be related to some trace amounts of impurity in the sample.

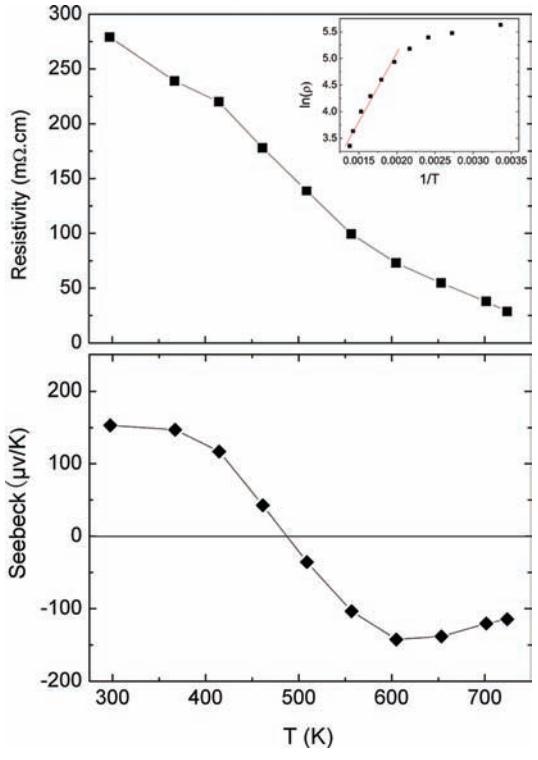

Figure 8. Temperature-dependent electrical resistivity (top) and Seebeck coefficient (bottom) data for $Eu_5Sn_2As_6$ simultaneously in a temperature range from 300 to 780 K under a He atmosphere.

semiconductor, which is supported by the theoretical calculations discussed above. When the high-temperature data (above 500 K) were fitted to an intrinsic semiconducting behavior [$\rho = \rho_0 \exp(E_g/2k_BT)$], a band gap of 0.45 eV for $Eu_5Sn_2As_6$ was obtained, which is a little smaller than that of undoped $Ca_5Al_2Sb_6$ (0.5 eV); the latter also showed relatively poorer electrical conductivity.[12] Generally, it is more reasonable that the antimonide compound has a smaller band gap than its arsenide analogue. However, if rare-earth metals are introduced, the band gap can be reduced greatly. This has been well proved in our previous work on the A_2CdPn_2 system (A = Ca, Sr, Eu; Pn = P, As), in which the band gaps for Ca_2CdAs_2 and Eu_2CdAs_2 are about 1.0 and 0.29 eV, respectively.[17] The Seebeck coefficient of $Eu_5Sn_2As_6$ is positive at room temperature; however, it changes to negative values at high temperature (above 500 K). This possibly suggests that both holes and electrons play an important role in governing the electrical transport properties of $Eu_5Sn_2As_6$. Such a behavior has also been frequently observed in the intrinsic semiconductors as well as intermetallics.[54−56] The Seebeck coefficient of $Eu_5Sn_2As_6$ is pretty large, about 100 μV/K at room temperature and −150 μV/K at 600 K, which is within the same magnitude as some known thermoelectric materials, such as $Ca_5Al_2Sb_6$,[12] $Yb_{11}InSb_9$, $Yb_{11}GaSb_9$,[57] and $Yb_{14}MnSb_{11}$,[15] to name just a few.

The thermal conductivity of $Eu_5Sn_2As_6$ is also very low, which is not surprising because its crystal structure highly resembles that of $Ca_5Al_2Sb_6$.[12] The measured total thermal conductivity κ_t is presented in Figure 9 (top), and the

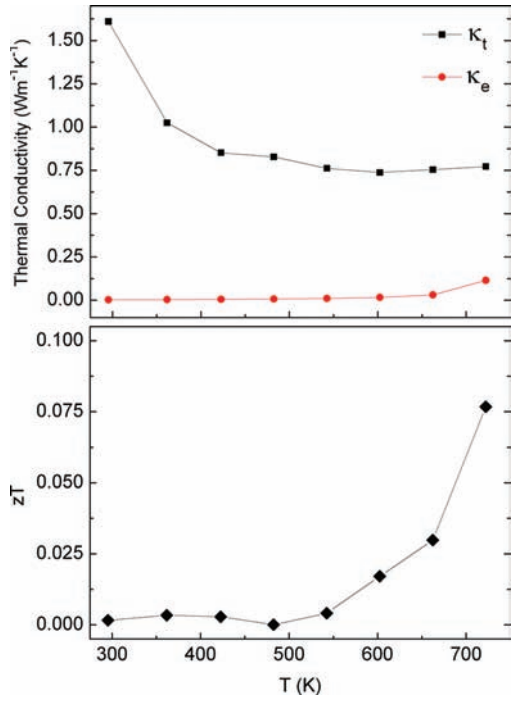

Figure 9. Thermal conductivity data (top) and estimated figure of merit (bottom) for $Eu_5Sn_2As_6$. The electronic thermal conductivity κ_e was also plotted on the same temperature scale for a comparison with the total thermal conductivity κ_t.

electronic thermal conductivity κ_e was estimated using the Wiedemann−Franz relationship ($\kappa_e = LT/\rho$). The results demonstrated an overwhelming contribution from the lattice thermal conductivity κ_l because κ_e was almost negligible in contrast to κ_t. It is not surprising that $Eu_5Sn_2As_6$ does not show very satisfying thermoelectric performance because of the poor electrical conductivity; the calculated zT values are less than 0.1 in the measured temperature range, as indicated in Figure 9 (bottom). However, the results are still promising, and the figure of merit is comparable with that of undoped $Ca_5Al_2Sb_6$.[12] In order to achieve higher zT, a doping strategy similar to that

dx.doi.org/10.1021/ic300308w | Inorg. Chem. 2012, 51, 5771−5778

applied in the $Ca_{5-x}Na_xAl_2Sb_6$ series is necessary, which can help tune the carrier concentration and improve the electrical conductivity as well.

CONCLUSIONS

In conclusion, two new ternary Zintl phases, $Sr_5Sn_2As_6$ and $Eu_5Sn_2As_6$, have been synthesized and characterized. The close structural relationship between $Eu_5Sn_2As_6$ and $Ca_5Al_2Sb_6$ has stimulated our interest in the thermoelectric properties of $Eu_5Sn_2As_6$, which proved to exhibit electrical and thermal transport properties comparable to those of undoped $Ca_5Al_2Sb_6$. Theoretical calculations involving these two subtly different structure types, here exemplified by $Ca_5Ga_2As_6$ and $Sr_5Sn_2As_6$, suggest different electronic band structures and electron occupation states of As p orbitals around the Fermi level, which also help to understand the different behaviors of the Seebeck coefficient related to $Ca_5Al_2Sb_6$ and $Eu_5Sn_2As_6$. More work aimed at enhancing the thermoelectric performance of this series of new materials by applying various doping strategies is still in progress.

ASSOCIATED CONTENT

Supporting Information

X-ray crystallographic files in CIF format for all title compounds and representative powder diffraction patterns for $Eu_5Sn_2As_6$ before and after SPS treatments. This material is available free of charge via the Internet at http://pubs.acs.org.

AUTHOR INFORMATION

Corresponding Author

*E-mail: shqxia@sdu.edu.cn (S.-Q.X.), txt@sdu.edu.cn(X.-T.T.). Phone: (531) 883-62519 (S.-Q.X.), (531) 883-64963 (X.-T.T.). Fax: (531) 883-62519 (S.-Q.X.), (531) 883-64864 (X.-T.T.).

Notes

The authors declare no competing financial interest.

ACKNOWLEDGMENTS

S.-Q.X. acknowledges financial support of the start-up grants from the Shandong University, the State Key Laboratory of Crystal Materials, and the Scientific Research Foundation for the Returned Overseas Chinese Scholars, State Education Ministry. This work is also sponsored by the National Natural Science Foundation of China (Grants 20901047, 51021062, and 50990061), the Shandong Provincial Natural Science Foundation (Grant ZR2010BM003), and the 973 Program of the People's Republic of China (Grant 2010CB630702). Much thanks goes to Prof. Ling Chen from FJIRSM, CAS, for measurements of the Seebeck coefficient and electrical conductivity.

REFERENCES

(1) *Chemistry, Structure and Bonding of Zintl Phases and Ions*; Kauzlarich, S. M., Ed.; VCH Publishers: New York, 1996; and references cited therein.
(2) Papoian, G. A.; Hoffmann, R. *Angew. Chem., Int. Ed.* **2000**, *39*, 2408−2488.
(3) Corbett, J. D. *Angew. Chem., Int. Ed.* **2000**, *39*, 670−690.
(4) Snyder, G. J.; Toberer, E. S. *Nat. Mater.* **2008**, *7*, 105−114.
(5) Toberer, E. S.; May, A. F.; Snyder, G. J. *Chem. Mater.* **2010**, *22*, 624−634.
(6) Kauzlarich, S. M.; Brown, S. R.; Snyder, G. J. *Dalton Trans.* **2007**, *21*, 2099−2107.
(7) Xia, S. Q.; Bobev, S. *J. Am. Chem. Soc.* **2007**, *129*, 4049−4057.
(8) Zintl, E. *Angew. Chem.* **1939**, *52*, 1−6.
(9) Wade, K. *Adv. Inorg. Chem. Radiochem.* **1976**, *18*, 1−66.
(10) Nesper, R. *Angew. Chem., Int. Ed. Engl.* **1991**, *30*, 789−817.
(11) Zevalkink, A.; Toberer, E. S.; Zeier, W.; Flage-Larsen, E.; Snyder, G. J. *Energy Environ. Sci.* **2011**, *4*, 510−518.
(12) Toberer, E. S.; Zevalkink, A.; Crisosto, N.; Snyder, G. J. *Adv. Funct. Mater.* **2010**, *20*, 4375−4380.
(13) Sales, B. C.; Chakoumakos, B. C.; Jin, R.; Thompson, J. R.; Mandrus, D. *Phys. Rev. B* **2001**, *63*, 245113.
(14) Gascoin, F.; Ottensmann, S.; Stark, D.; Haile, S. M.; Snyder, G. J. *Adv. Funct. Mater.* **2005**, *15*, 1860−1864.
(15) Brown, S. R.; Kauzlarich, S. M.; Gascoin, F.; Snyder, G. J. *Chem. Mater.* **2006**, *18*, 1873−1877.
(16) Zevalkink, A.; Toberer, E. S.; Bleith, T.; Flage-Larsen, E.; Snyder, G. J. *J. Appl. Phys.* **2011**, *110*, 013721.
(17) Wang, J.; Yang, M.; Pan, M.-Y.; Xia, S.-Q.; Tao, X.-T.; He, H.; Darone, G.; Bobev, S. *Inorg. Chem.* **2011**, *50*, 8020−8027.
(18) Eisenmann, B.; Klein, J. *Z. Anorg. Allg. Chem.* **1991**, *598*, 93−102.
(19) Asbrand, M.; Eisenmann, B.; Klein, J. *Z. Anorg. Allg. Chem.* **1995**, *621*, 576−582.
(20) Lam, R.; Mar, A. *Solid State Sci.* **2001**, *3*, 503−512.
(21) Eisenmann, B.; Jordan, H.; Schäfer, H. *Z. Naturforsch., Teil B: Anorg. Chem.* **1984**, *39*, 1151−1153.
(22) Eisenmann, B.; Jordan, H.; Schäfer, H. *Z. Anorg. Allg. Chem.* **1985**, *530*, 74−78.
(23) Eisenmann, B.; Jordan, H.; Schäfer, H. *J. Less Common Met.* **1986**, *116*, 251−258.
(24) *Bruker APEX2*; Bruker AXS Inc.: Madison, WI, 2005.
(25) Sheldrick, G. M. *SHELXTL*; University of Göttingen: Göttingen, Germany, 2001.
(26) Parthé, E.; Gelato, L. M. *Acta Crystallogr.* **1984**, *A40*, 169.
(27) Gelato, L. M.; Parthé, E. *J. Appl. Crystallogr.* **1987**, *20*, 139.
(28) Brown, S. R.; Toberer, E. S.; Ikeda, T.; Cox, C. A.; Gascoin, F.; Kauzlarich, S. M.; Snyder, G. J. *Chem. Mater.* **2008**, *20*, 3412−3419.
(29) Madsen, G. K. H.; Blaha, P.; Schwarz, K.; Sjöstedt, E.; Nordström, L. *Phys. Rev. B* **2001**, *64*, 195134.
(30) Schwarz, K.; Blaha, P.; Madsen, G. K. H. *Comput. Phys. Commun.* **2002**, *147*, 71.
(31) Blaha, P.; Schwarz, K.; Madsen, G. K. H.; Kvasnicka, D.; Luitz, J. *WIEN2k, An Augmented Plane Wave + Local Orbitals Program for Calculating Crystal Properties*; Technische Universität: Vienna, Austria, 2001.
(32) Perdew, J. P.; Burke, S.; Ernzerhof, M. *Phys. Rev. Lett.* **1996**, *77*, 3865.
(33) Andersen, O. K. *Phys. Rev. B* **1975**, *12*, 3060.
(34) Andersen, O. K.; Jepsen, O. *Phys. Rev. Lett.* **1984**, *53*, 2571.
(35) Andersen, O. K.; Jepsen, O.; Glötzel, D. In *Highlights of condensed matter theory*; Bassani, F., Fumi, F., Tosi, M. P., Eds.; North Holland: New York, 1985.
(36) Andersen, O. K. *Phys. Rev. B* **1986**, *34*, 2439.
(37) Skriver, H. L. *The LMTO Method*; Springer: Berlin, Germany, 1984.
(38) Jepsen, O.; Andersen, O. K. *The Stuttgart TB-LMTO Program, Version 4.7*, Max-Planck-Institut für Festkörperforschung: Stuttgart, Germany, 1994.
(39) Von Barth, U.; Hedin, L. *J. Phys. C* **1972**, *5*, 1629.
(40) Koelling, D. D.; Harmon, B. N. *J. Phys. C* **1977**, *10*, 3107.
(41) Jepsen, O.; Andersen, O. K. *Z. Phys. B* **1995**, *97*, 35.
(42) Lambrecht, W. R. L.; Andersen, O. K. *Phys. Rev. B* **1986**, *34*, 2439.
(43) Blöchl, P. E.; Jepsen, O.; Andersen, O. K. *Phys. Rev. B* **1994**, *49*, 16223.
(44) Verdier, P.; L'Haridon, P.; Mounaye, M.; Laurent, Y. *Acta Crystallogr., Sect. B* **1976**, *32*, 726−728.
(45) Cordier, G.; Schäfer, H.; Stelter, M. *Z. Naturforsch.* **1984**, *39B*, 727−732.

(46) Cordier, G.; Schäfer, H.; Stelter, M. *Z. Naturforsch.* **1985**, *40B*, 5−8.
(47) Cordier, G.; Schäfer, H.; Stelter, M. *Z. Naturforsch.* **1985**, *40B*, 1100−1104.
(48) Grey, I. E.; Steinfink, H. *Inorg. Chem.* **1971**, *10*, 691−696.
(49) Greaney, M. A.; Ramanujachary, K. V.; Teweldemedhin, Z.; Greenblatt, M. *J. Solid State Chem.* **1993**, *107*, 554−562.
(50) Mewis, A. *Z. Naturforsch.* **1980**, *35B*, 939−941.
(51) Xia, S.-Q.; Bobev, S. *Inorg. Chem.* **2008**, *47*, 1919−1921.
(52) Kim, H.; Condron, C. L.; Holm, A. P.; Kauzlarich, S. M. *J. Am. Chem. Soc.* **2000**, *122*, 10720−10721.
(53) Goforth, A. M.; Hope, H.; Condron, C. L.; Kauzlarich, S. M.; Jensen, N.; Klavins, P.; MaQuilon, S.; Fisk, Z. *Chem. Mater.* **2009**, *21*, 4480−4489.
(54) Brown, S. R.; Kauzlarich, S. M.; Gascoin, F.; Snyder, G. J. *J. Solid State Chem.* **2007**, *180*, 1414−1420.
(55) Amato, A.; Jaccard, D.; Sierro, J.; Lapierre, F.; Haen, P.; Lejay, P.; Flouquet, J. *J. Magn. Magn. Mater.* **1988**, *76−77*, 263−264.
(56) Oeschler, N.; Deppe, M.; Hartmann, S.; Caroca-Canales, N.; Geibel, C.; Steglich, F. *J. Phys.: Conf. Ser.* **2010**, *200*, 012148.
(57) Yi, T. H.; Cox, C. A.; Toberer, E. S.; Snyder, G. J.; Kauzlarich, S. M. *Chem. Mater.* **2010**, *22*, 935−941.